Microstructural investigation of oxidized Ni/Au ohmic contact to p-type GaN

Li-Chien Chen, Fu-Rong Chen, Ji-Jung Kai, Li Chang, Jin-Kuo Ho, Charng-Shyang Jong, Chien C. Chiu, Chao-Nien Huang, Chin-Yuen Chen, and Kwang-Kuo Shih

Articles you may be interested in

Correlation between microstructure and temperature dependent electrical behavior of annealed Ti/Al/Ni/Au Ohmic contacts to AlGaN/GaN heterostructures
Appl. Phys. Lett. **103**, 201604 (2013); 10.1063/1.4828839

Chemical, electrical, and structural properties of Ni/Au contacts on chemical vapor cleaned p-type GaN
J. Appl. Phys. **91**, 9151 (2002); 10.1063/1.1471578

Investigation of oxidation mechanism for ohmic formation in Ni/Au contacts to p-type GaN layers
Appl. Phys. Lett. **79**, 3815 (2001); 10.1063/1.1425065

Correlation of contact resistance with microstructure for Au/Ni/Al/Ti/AlGaN/GaN ohmic contacts using transmission electron microscopy
J. Appl. Phys. **89**, 3143 (2001); 10.1063/1.1347003

Oxidized Ni/Pt and Ni/Au ohmic contacts to p-type GaN
Appl. Phys. Lett. **76**, 3703 (2000); 10.1063/1.126755

Microstructural investigation of oxidized Ni/Au ohmic contact to *p*-type GaN

Li-Chien Chen,[a)] Fu-Rong Chen, and Ji-Jung Kai
Department of Engineering and System Science, National Tsing Hua University Hsinchu, Taiwan 300, Republic of China

Li Chang
Department of Material Science and Engineering, National Chiao Tung University, Hsinchu, Taiwan 300, Republic of China

Jin-Kuo Ho, Charng-Shyang Jong, Chien C. Chiu, Chao-Nien Huang, Chin-Yuen Chen, and Kwang-Kuo Shih
Opto-Electronics and Systems Laboratories, Industrial Technology Research Institute, Chutung, Hsinchu, Taiwan 310, Republic of China

The microstructure of oxidized Ni/Au films on *p*-GaN was examined to elucidate the formation of a low resistance ohmic contact to *p*-GaN with a field-emission gun transmission electron microscope in conjunction with composition analyses. The *p*-GaN/Ni/Au samples were heat treated at 500 °C in air mainly composed of a mixture of crystalline NiO, Au, and amorphous Ni–Ga–O phases. Small voids adjacent to the *p*-GaN film were also observed. The as-deposited Au film converted into discontinuous islands containing small amounts of Ni that connect with *p*-GaN. NiO formed a continuous film at the surface that covers the Au islands and the amorphous Ni–Ga–O phases. Moreover, NiO partially contacts *p*-GaN as well as Au islands and the amorphous Ni–Ga–O phase. The orientation relationship of the crystalline NiO, Au-rich islands, and *p*-GaN film was identified as NiO(111)//Au(11$\bar{1}$)//GaN(0002) and NiO[1$\bar{1}$0]//Au[1$\bar{1}$0]//GaN[11$\bar{2}$0]. The results suggested that Ni atoms diffuse through the Au layer onto the surface and react with oxygen to form NiO, whereas Au atoms diffuse towards the inside to form a Au–Ni alloy. The microstructural examination indicated that the crystalline NiO and/or the amorphous Ni–Ga–O phases may significantly affect the low resistance ohmic contact to *p*-GaN. © *1999 American Institute of Physics.* [S0021-8979(99)05219-6]

I. INTRODUCTION

The gallium nitride based semiconductor is one of the most promising materials for optoelectronic applications such as light emitting diodes (LEDs) and laser diodes (LDs) in the blue and ultraviolet ranges. The recent development of high quality GaN crystalline film has resulted in rapid progress in the development of high brightness blue LEDs[1] and continuous wave LDs at room temperature.[2] However, such optoelectronic devices need low resistance ohmic contacts to both *n*- and *p*-type GaN to enhance their performance. Several approaches for constructing low resistance ohmic contacts to *n*-type GaN have been studied.[3–8] The most widely used ohmic contacts to *n*-type GaN are based on an Al/Ti bilayer.[3–6] Related investigations proposed the formation of reaction phases such as Al–Ti intermetallics,[3,4] TiN,[4,5] and AlN (Refs. 5 and 6) to induce low specific contact resistance ranging between 10^{-6} and $10^{-7}\,\Omega\,\text{cm}^2$. In contrast to the great amount of attention paid to *n*-type GaN contact, low resistance ohmic contact to *p*-type GaN has meet with less success. Specific contact resistance to *p*-GaN was restricted to 10^{-2}–$10^{-3}\,\Omega\,\text{cm}^2$. Such a high value is insufficient for high performance device applications. The

major restrictions in achieving low resistance ohmic contacts to *p*-type GaN is that the carrier concentration of *p*-GaN cannot be increased to a degenerated level, and a practical metal with a high work function is not available. The carrier concentration of *p*-GaN prepared by epitaxial growth is generally limited to about $10^{18}\,\text{cm}^{-3}$.[9,10] Other methods, e.g., diffusion[11,12] and ion implantion,[13–16] were also applied to increase the carrier concentration. However, no significant improvement has been achieved. Thus, metallic materials with a high work function are expected to alleviate the resistance. Multilayer metallic films with a high work function, such as Ni/Au,[17–21] Pt/Au,[22] and Pt/Ni/Au,[23] are extensively used as contacts to *p*-type GaN.

Recently Ho *et al.*[21] successfully developed a contact to *p*-type GaN with a specific contact resistance lower than $1 \times 10^{-4}\,\Omega\,\text{cm}^2$ using an oxidizing Ni (10 nm)/Au (5 nm) metallization scheme.[21] This value is approximately one to two orders of magnitude lower than any contact resistance previously reported. They attributed the low resistance ohmic contact to the formation of NiO. These excellent electrical properties promoted this detailed investigation of the microstructure of as-deposited and oxidized Ni/Au films on *p*-GaN to analyze the phase evolution of alloys that correlate with low contact resistance to *p*-type GaN. Furthermore, the

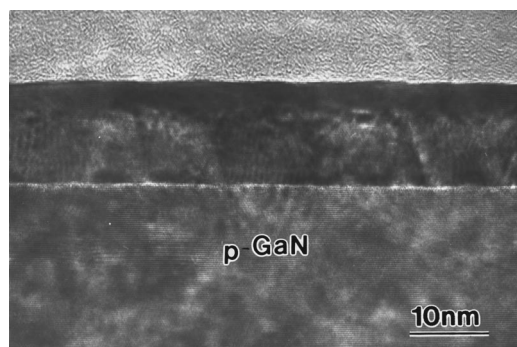a)Electronic mail: d843532@oz.nthu.edu.tw

FIG. 1. Typical cross-sectional TEM image of the as-deposited *p*-GaN/Ni/Au sample.

reaction mechanism and diffusion behavior are also discussed in this study.

II. EXPERIMENT

Sapphire/undoped GaN (2 μm)/Mg-doped GaN (2 μm) samples were prepared by metalorganic chemical vapor deposition (MOCVD). Trimethylgallium and ammonia were used as the sources of Ga and N, respectively. The sapphire substrates were cleaned with organic solvents before they were loaded into the MOCVD system. A low temperature GaN nucleation layer was initially grown on the sapphire substrates, and 2 μm undoped GaN and 2 μm Mg-doped GaN were subsequently grown at about 1000 °C. Heat treatment of the GaN samples in N_2 atmosphere at suitable temperature was used to activate the Mg atoms to the *p*-type dopant. The results of Hall measurement showed that the hole concentration of *p*-GaN was 2×10^{17} cm^{-3}. Prior to metal deposition, the samples were etched with HCl:H_2O = 1:1 for 1 min to remove native oxide, and then 10 nm Ni and 5 nm Au were deposited on the *p*-type GaN as metal contacts by electron beam evaporation under a base pressure that was lower than 3×10^{-6} Torr. We then oxidized the as-deposited Ni/Au sample at 500 °C in air for 10 min to induce interdiffusion of the bi layer metals (Ni and Au) and reaction with oxygen. Thus a low resistance ohmic contact to *p*-GaN was obtained.

Microstructural and compositional analyses were performed using a JEOL 2010F field emission gun transmission electron microscope (FE-TEM) equipped with an Oxford energy dispersive x-ray spectrometer (EDS) and a Gatan image filter (GIF). Elemental mappings and high-resolution electron energy loss spectroscopy (EELS) spectra were both obtained by the GIF system. Crystal structure identification, EDS, and EELS were carried out using a 0.5 nm nanobeam probe. Cross-sectional TEM samples were prepared by the tripod polishing method. Then the TEM samples were mounted on Cu grids and ion milling followed.

III. RESULTS AND DISCUSSION

The as-deposited Ni and Au films were polycrystalline with a small grain size of few nanometers, as depicted in Fig. 1. The Ni layer was grown in a column-like structure on *p*-GaN with the preferred orientation, Ni(002)//GaN(0002).
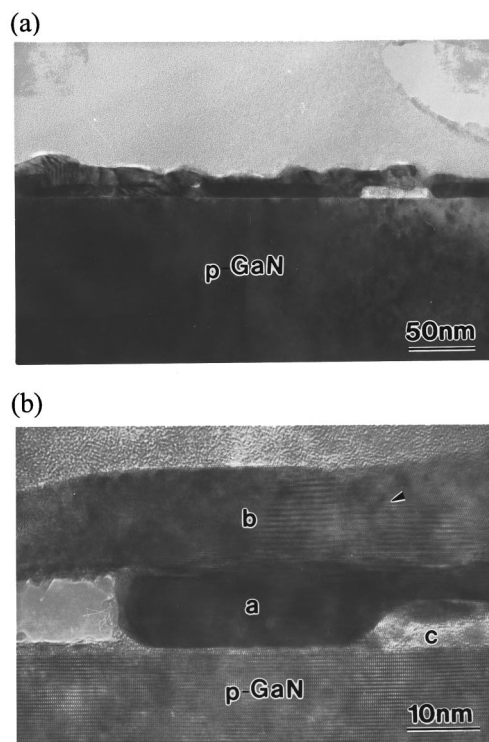

FIG. 2. TEM micographs of *p*-GaN/Ni/Au samples after an oxidizing treatment at 500 °C for 10 min in air. (a) Low magnification image and (b) high-resolution image.

The subsequently deposited Au layer was built epitaxially on the Ni layer, and had an ambiguous interface. No interlayer between Ni and *p*-GaN was observed. This finding indicates that the sample precleaning and subsequent deposition caused no contamination or reaction between the interface of Ni and *p*-GaN; this is different from the results reported by Bermudez *et al.*,[24] who observed reaction even near room temperature. However, in current–voltage measurement, the as-deposited sample showed a rectifying characterisic.[21] Heat treatment of the as-deposited samples in N_2 or in forming gas did not change the rectifying characteristic.

After an oxidizing treatment at 500 °C in air, the bilayer metals reacted with oxygen and were transformed into a new microstructure that makes the contact ohmic with low interface resistance.[21] Figure 2(a) displays a typical microstructure of the oxidized sample in cross-sectional view. Discrete crystalline islands with darker contrast were observed; the amorphous phase and voids existed among the crystalline grains. A nonuniform crystalline thin film with an uneven surface covered these features. High-resolution TEM and EDS analyses were performed to examine in detail the composition and microstructure of these phases. These results are shown in Figs. 2(b), 3, and 4. Figure 2(b) is a magnified micrograph of the typical oxidized sample. The EDS spectra and the diffraction patterns, depicted in Figs. 3 and 4, respectively, correspond to the points marked ''a,'' ''b,'' and ''c'' in Fig. 2(b). Both the EDS spectra and the diffraction patterns were obtained using a 0.5 nm electron probe. Figure 3(a) presents the EDS spectrum from point ''a'' of the discontinuous island of Fig. 2(b); this spectrum indicates that the island primarily consists of Au, with a small amount of
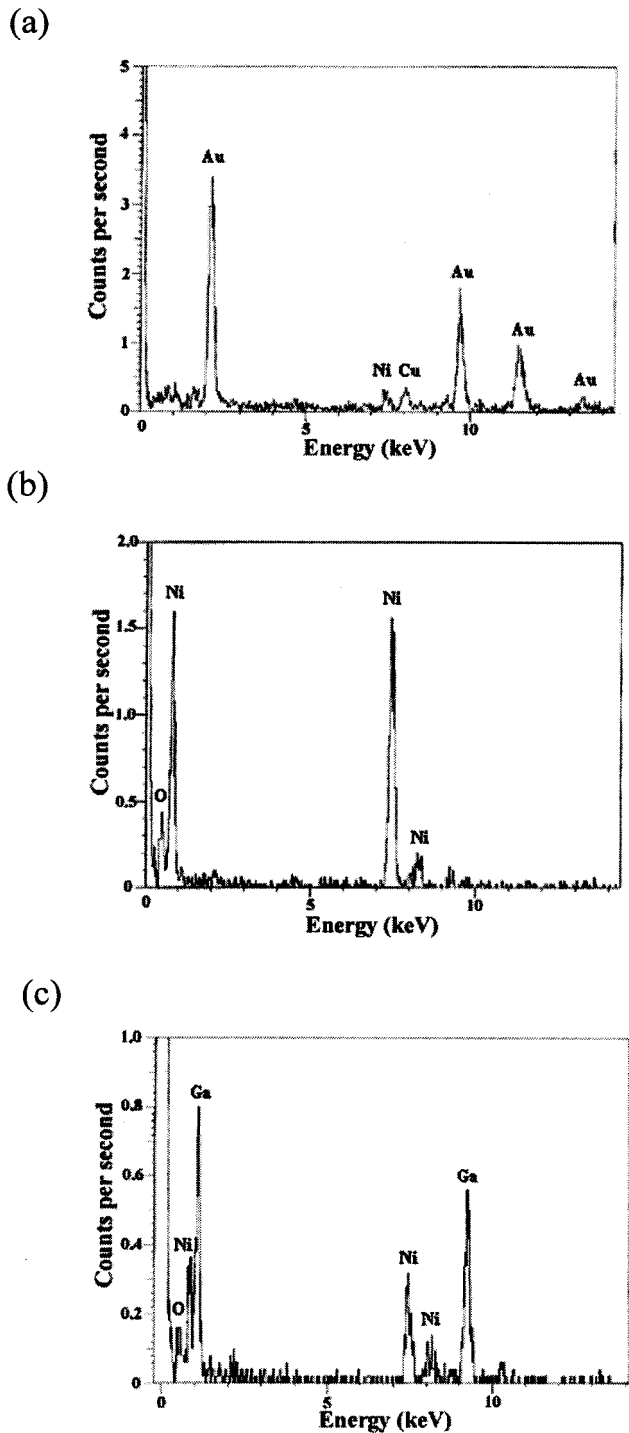
(a)

(b)

(c)

FIG. 3. EDS spectra obtained from points (a) ''a,'' (b) ''b,'' and (c) ''c'' of Fig. 2(b), respectively.

(a)

(b)

(c)

FIG. 4. Nanobeam diffraction patterns obtained from points (a) ''a'' and (b) ''b'' of Fig. 2(b), and from (c) the *p*-GaN film, respectively. The diffraction patterns identify the phases as (a) Au, (b) NiO with a face-centered-cubic structure in the [110] zone axis, and (c) GaN with a close-packed-hexagonal structure in the [1120] zone axis.

Ni. Figure 4(a) shows the diffraction pattern from the same point that is consistent with the Au structure. The results identify the discrete islands as Au-rich grains. Conversely, the crystalline film above the Au islands was mainly composed of Ni and O, as illustrated by the EDS spectrum in Fig. 3(b), which was obtained from point ''b'' in Fig. 2(b). This film was further confirmed as being a face-centered-cubic NiO phase by a nanobeam diffraction pattern depicted in Fig. 4(b). Some inclined twins were observed in the crystalline NiO film, as indicated by an arrow in Fig. 2(b). These de-
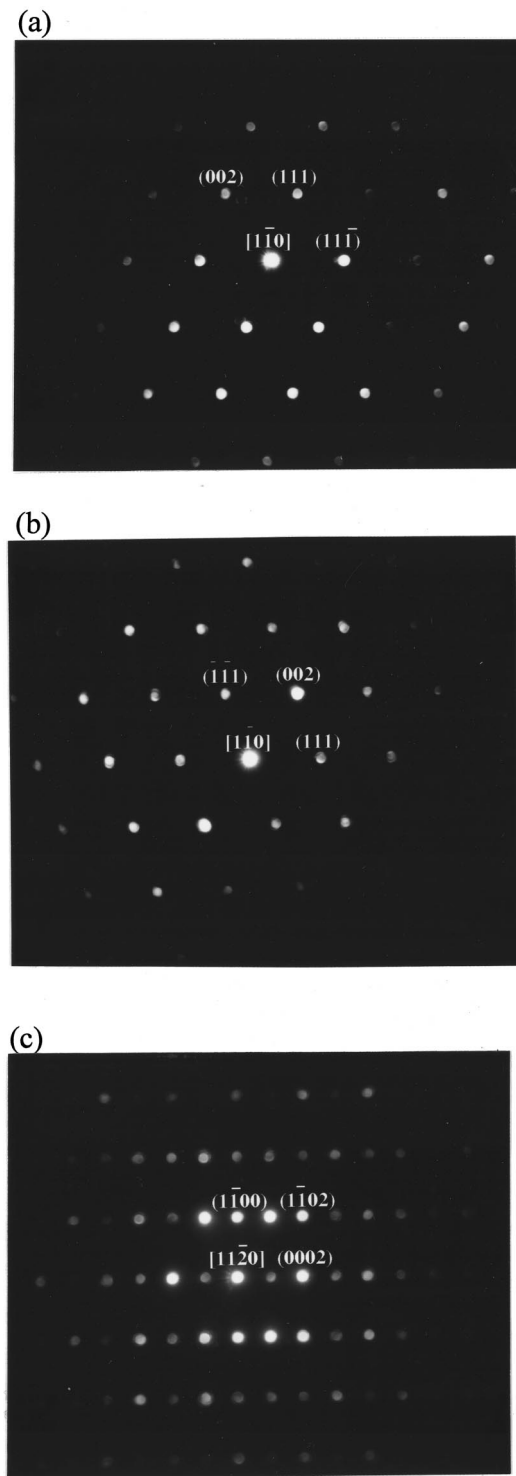
fects are commonly seen in the face-centered-cubic structure. The EDS analysis, illustrated in Fig. 3(c) from point ''c'' of Fig. 2(b), displays the amorphous regions consisting of a relatively larger amount of Ga as well as Ni and O. The EDS semiquantification analysis indicated that the Ga:Ni atomic ratio is about 2:1. The orientation relationships among
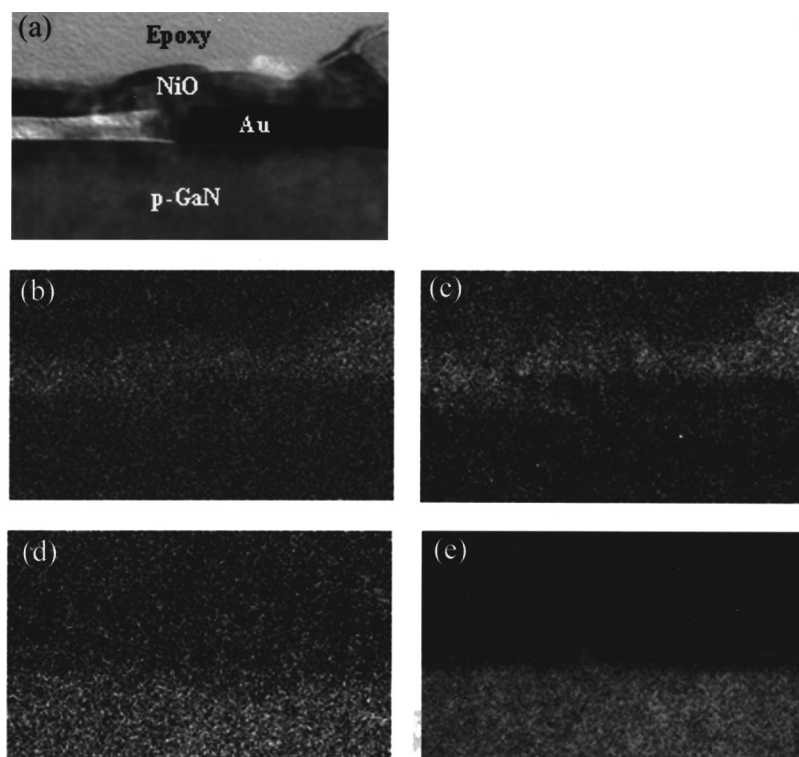
FIG. 5. Electron energy filtering mapping of the oxidized Ni/Au film. (a) Zero loss image with a 50 eV slit width, (b) Ni mapping, (c) O mapping, (d) Ga mapping, and (e) N mapping.

the NiO film, the Au islands, and the *p*-GaN are determined from the nanobeam diffraction patterns illustrated in Fig. 4. These orientation relationships are given as NiO(111)‖Au(11$\bar{1}$)‖GaN‖(0002) and NiO[1$\bar{1}$0]‖Au[1$\bar{1}$0]‖GaN[11$\bar{2}$0].

The preceding results give the following implications. During annealing at 500 °C in air, interdiffusion of Ni and Au atoms occurred. It is conceivable that grain boundaries[25] of the as-deposited Au film may serve as quick diffusion channels for outdiffusion of Ni atoms to the surface at this temperature. The driving force for the Ni atoms diffusing out through the Au layer results from the stronger affinity of Ni to O than that of Au to O. During the outdiffusion of Ni atoms to the surface, interdiffusion between Ni and Au atoms at the interface also occurred, and this could lead to the formation of the Ni–Au alloy. According to the Ni–Au phase diagram,[26] the equilibrium concentration of the Au–Ni alloy at 500 °C is 5% Ni–Au or 93% Ni–Au as a result of the miscibility gap. The EDS quantification indicates that the concentration of Ni in Au-rich islands is much less than 5% or even that there was no Ni detected in the Au islands. This suggests that the Ni in the Ni–Au alloy is steadily consumed as a consequence of the oxidation of Ni at the surface. Thereby, little Ni is left in the Au-rich islands and the NiO film is constructed on the top of the Au-rich islands.

After oxidation, the Au-rich islands were sandwiched by the NiO and GaN, which results in forming two new interfaces of Au/NiO and GaN/Au. The equilibrium contact angle between the Au islands with GaN was about 120°–140° due to the balance of surface energy among the GaN, and NiO or the amorphous Ni–Ga–O phase. The average thickness of Au-rich islands also changed to approximately 10 nm, that is, to double the as-deposited thickness. Thereby, the small
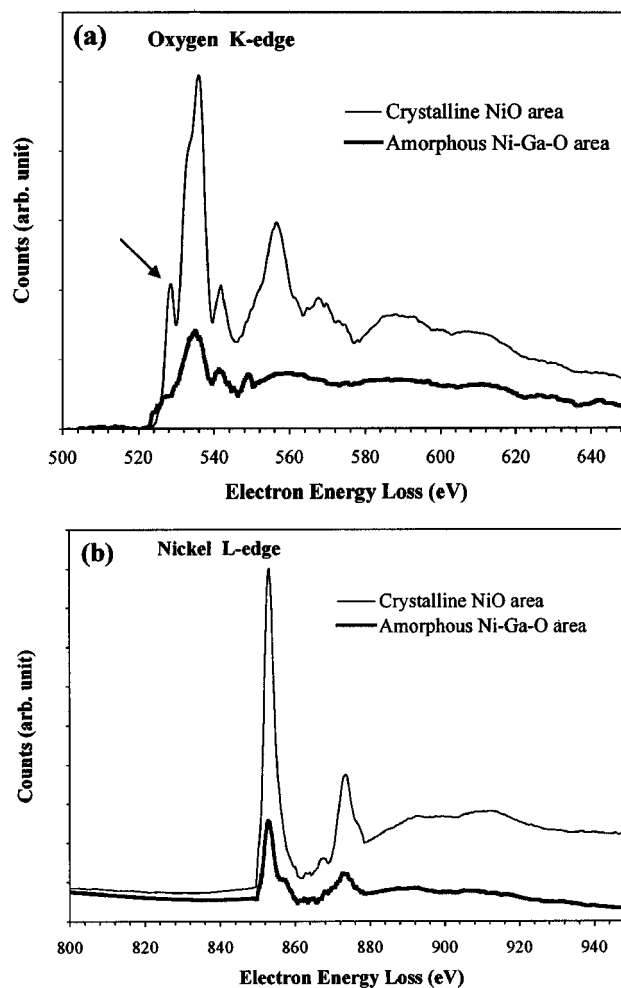

FIG. 6. Electron energy loss spectra of crystalline NiO and the amorphous Ni–Ga–O phase. (a) Oxygen *K* edge and (b) Ni *L* edge.
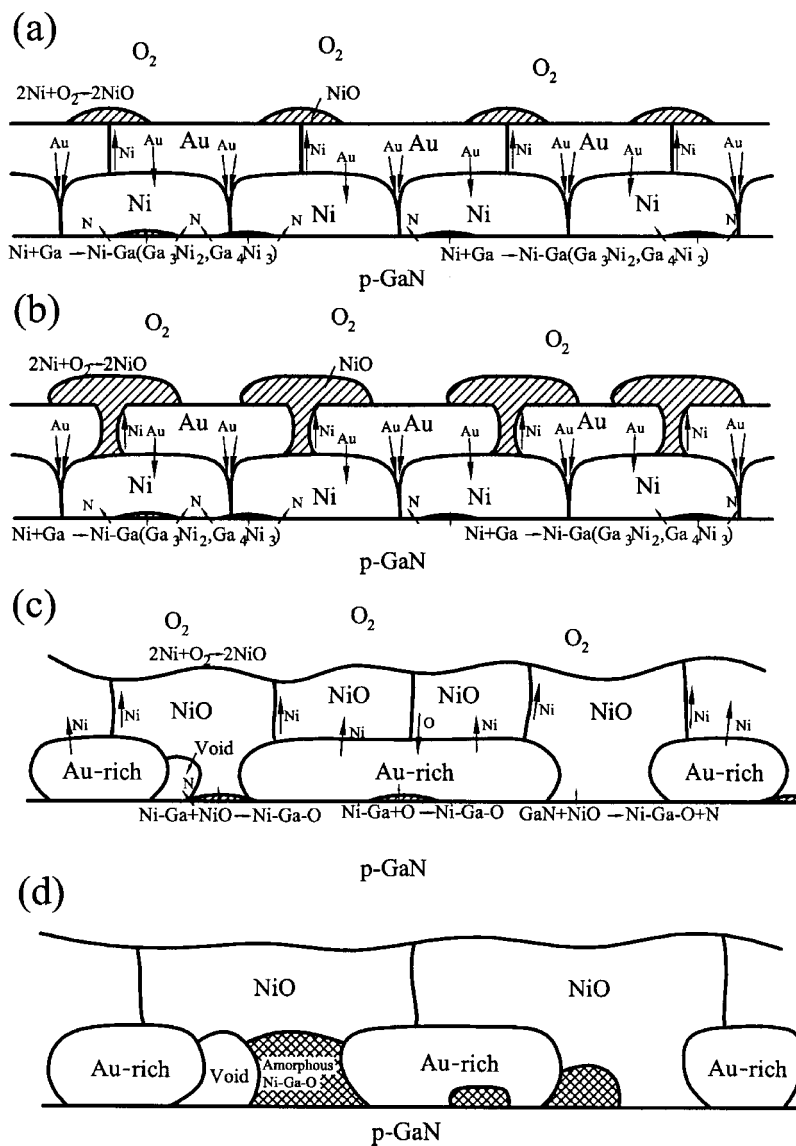
FIG. 7. Schematic illustration of the reaction mechanism and diffusion behavior during the oxidation of *p*-GaN/Ni/Au. (a) Early stage of oxidation reaction, (b) pronounced interdiffusion and crystalline NiO grow up to separate the Au–Ni alloy into discrete islands, (c) Au-rich islands building epitaxially on *p*-GaN and three possible reactions producing Ni–Ga–O phases, and (d) oxidized contact scheme with optimum phase distribution.

voids observed in Fig. 2(b) may have appeared as a consequence of conserving the constant volume of Au. The formation of voids reduced the contact area to *p*-GaN after oxidation, which could degrade the contact performance.

The energy filtering mapping images, depicted in Fig. 5, provided an overall picture of the compositional distribution of the oxidation process. Figures 5(a)–5(e) display the zero loss image, and the Ni, O, Ga, and N elemental mappings, respectively. The width of the selected energy window ranged from 30 to 50 eV according to the energy loss. The energy window was centered on the energy loss levels of 855, 532, 1115, and 400 eV for Ni, O, Ga, and N mappings, respectively. The bright contrast in the Ni and O mappings was consistent with the EDS analysis (Fig. 3); this bright contrast was identified as the crystalline NiO and amorphous regions. On the other hand, Au islands showed darker contrast in these two mappings. Furthermore, the Ga mapping displayed a diffusive Ga interface, in contrast to a sharper interface from N mapping. This suggests that GaN dissociated into Ga and N after the heat treatment. The Ga atoms are distributed near the interface, but the N atoms might

diffuse out or join the voids. Because the intensity of the Ga signal in the amorphous region of the Ga mapping is comparable to the noise, no useful information could be extracted.

More atomic information of crystalline NiO and the amorphous Ni–Ga–O phase was obtained from EELS, as depicted in Fig. 6. The electron core energy loss of the oxygen *K* edge is near 532 eV, and that from the Ni *L* edge is about 855 eV. Figures 6(a) and 6(b) present the oxygen *K*-edge electron energy loss near edge structures (ELNES) following background subtraction and the Ni *L*-edge ELNES, respectively. The oxygen *K*-edge ELNES of crystalline NiO is obviously different from that of the amorphous Ni–Ga–O phase. The initial 5–10 eV from the threshold of the oxygen spectra contains information on the O $2p$ orbital hybridizing with the Ni $3d$ levels.[27,28] The first edge of oxygen ELNES of the crystalline NiO, indicated by an arrow in Fig. 6(a), disappears in the amorphous Ni–Ga–O phase. This kind of edge is associated with the existence of unoccupied states of mixed O $2p$ with Ni $3d$ orbitals. Correspondingly, oscillations of 5 or 10 to about 30 eV from the threshold of

the ELNES reflect the local atomic environment. The difference in ELNES between the crystalline NiO film and the amorphous Ni–Ga–O phase indicates the change in atomic bonding and valence state. EELS quantification analysis also shows that the Ni:O ratio of amorphous Ni–Ga–O regions is 10% lower than that of the crystalline NiO area. The compositional distribution might also significantly influence the electric properties.

Consequently, we believe that, during oxidation, some Ni atoms initially diffuse into the Au layer, enriching at the grain boundaries and, then, propagate to the surface to react with oxygen to form NiO. At the same time, the Ni left behind reacts with GaN to form the Ni–Ga alloy, Ga_4Ni_3, and Ga_3Ni_2.[20,24] When the NiO grows down to contact the Ni/GaN reaction products, such as the Ni–Ga alloy, Ga_4Ni_3, and Ga_3Ni_2,[20,24] a new oxidation reaction again takes place and an amorphous Ni–Ga–O phase forms with the liberation of N_2 to air or to the voids. According to the preceding results, a reaction mechanism is proposed to interpret the oxidation behavior of the Ni/Au contact to *p*-GaN; it is illustrated in Fig. 7. In the preliminary stage of oxidation, depicted in Fig. 7(a), Ni atoms start to diffuse out through the Au layer, primarily through grain boundaries, to react with oxygen and Au atoms that diffuse into the Ni layer to form the Au–Ni alloy. At the same time, the interfacial reaction between GaN and Ni may result in the formation of the Ga–Ni alloy and/or intermetallic compounds such as Ga_4Ni_3 and Ga_3Ni_2.[20,24] The progression of the diffusion, depicted in Fig. 7(b), further promotes the oxidation of Ni. The crystalline NiO grows up to separate the Au–Ni alloy into discrete islands. In the next stage, as illustrated in Fig. 7(c), the Au-rich islands migrate inside and epitaxially build on *p*-GaN while the NiO also grows down to contact the GaN or Ni–Ga products. Three possible reactions are attributed to the production of the amorphous Ni–Ga–O phase. First, the oxidation of GaN may occur when the NiO grows down to the interface. Second, the NiO may also react with the Ga–Ni alloy or with intermetallic compounds. Moreover, the oxygen atoms can diffuse through the boundaries between the Au-rich island and NiO or the amorphous Ni–Ga–O phase and react with the Ni–Ga product when the Ni–Ga product is under the Au-rich island. The nitrogen released from the reaction may diffuse out or join the voids and probably results in the loose structure of the amorphous phases. Ultimately, as demonstrated in Fig. 7(d), the discontinuous Au-rich islands, amorphous Ni–Ga–O phase, and some voids are sandwiched between crystalline NiO and the *p*-GaN film.

Although the stoichiometric crystalline NiO is an insulator, the NiO is found to be a *p*-type semiconductor while increasing Ni^{3+} ions by introducing Ni^{2+} vacancies and/or interstitial oxygen.[29] The low specific contact resistance of the oxidized Ni/Au metallization scheme was attributed to the high conductivity of Au islands and the low contact barrier of *p*-NiO to *p*-GaN.[21] However, this investigation discovered two products, the amorphous Ni–Ga–O phase and crystalline NiO contacting *p*-GaN. Whether one, or both, of these products is responsible for reducing the interface impedance still remains unclear at this time. Further studies

will continue to elucidate this formation of low resistance ohmic contact to *p*-GaN.

IV. CONCLUSIONS

Very low specific contact resistance to *p*-type GaN, lower than $1 \times 10^{-4} \, \Omega \, cm^2$, was attained by oxidizing Ni/Au bilayer metallization. The microstructural evolution of oxidized Ni (10 nm)/Au (5 nm) ohmic contact to *p*-type GaN was investigated. During oxidation, Ni diffused out through the Au layer to react with oxygen and thus form crystalline NiO. Ni was steadily consumed in the oxidizing reaction. The epitaxial orientation relationship of crystalline NiO, the Au-rich island, and *p*-type GaN were determined to be $NiO(111)\|Au(11\bar{1})\|GaN\|(0002)$ and $NiO[1\bar{1}0]\|Au[1\bar{1}0]\|GaN[11\bar{2}0]$. Crystalline NiO and the amorphous Ni–Ga–O phase were also found. EELS analysis demonstrated the different atomic bonding and valence states between crystalline NiO and the amorphous Ni–Ga–O phase. The results suggest that crystalline NiO and/or the amorphous Ni–Ga–O phase may play a significant role in lowering ohmic contact resistance to *p*-type GaN.

[1] S. Nakamura, T. Mukai, and M. Senoh, Appl. Phys. Lett. **64**, 1687 (1994).
[2] S. Nakamura, M. Senoh, S. Nagahama, N. Iwasa, T. Yamada, T. Matsushita, Y. Sugimoto, and H. Kiyoku, Jpn. J. Appl. Phys., Part 2 **36**, L1130 (1997).
[3] M. E. Lin, Z. Ma, F. Y. Huang, Z. F. Fan, L. H. Allen, and H. Morkoç, Appl. Phys. Lett. **64**, 1003 (1994).
[4] S. Ruvimov *et al.*, Appl. Phys. Lett. **69**, 1556 (1996).
[5] B. P. Luther, S. E. Mohney, T. N. Jackson, M. A. Khan, Q. Chen, and J. W. Yang, Appl. Phys. Lett. **70**, 57 (1997).
[6] B. P. Luther, S. E. Mohney, J. M. Delucca, and R. F. Karlicek, Jr., J. Electron. Mater. **27**, 196 (1998).
[7] Z. Fan, S. N. Mohammad, W. Kim, Ö. Aktas, A. E. Botchkarev, and H. Mokoç, Appl. Phys. Lett. **68**, 1672 (1996).
[8] J. Burn, K. Chu, W. A. Davis, W. J. Schaff, L. F. Eastman, and T. J. Eustis, Appl. Phys. Lett. **70**, 464 (1997).
[9] H. M. Ng, D. Doppalapudi, D. Korakakis, R. Singh, and T. D. Moustakas, J. Cryst. Growth **349**, 189 (1998).
[10] S. Nakamura and G. Fasol, *The Blue Laser Diode* (Springer, New York, 1997).
[11] T. Kim, M. C. Yoo, and T. Kim, Mater. Res. Soc. Symp. Proc. **449**, 1061 (1997).
[12] L. L. Smith, M. D. Bremser, E. P. Carlson, T. W. Weeks, Jr., Y. Huang, M. J. Kim, R. W. Carpenter, and R. F. Davis, Mater. Res. Soc. Symp. Proc. **395**, 861 (1996).
[13] B. Menschubg, C. Liu, B. Rauschenbach, K. Kornitzer, and W. Ritter, Mater. Sci. Eng., B **50**, 105 (1997).
[14] R. G. Wilson, C. B. Vartuli, C. R. Abernathy, S. J. Pearton, and J. M. Zavada, Solid-State Electron. **38**, 1329 (1995).
[15] J. C. Zolper, R. G. Wilson, S. J. Pearton, and R. A. Stall, Appl. Phys. Lett. **68**, 1945 (1996).
[16] M. Rubin, N. Newman, J. S. Chan, T. C. Fu, and J. T. Ross, Appl. Phys. Lett. **64**, 64 (1994).
[17] G. Mohs, B. Fluegel, H. Giessen, H. Tajalli, and N. Peyghambarian, Appl. Phys. Lett. **67**, 1515 (1995).
[18] S. Nakamura, M. Senoh, S. Nagaham, N. Iwasa, T. Matsushuta, H. Kiyiku, and Y. Sugimoto, Appl. Phys. Lett. **68**, 3269 (1996).
[19] H. Ishikawa, S. Kobayashi, Y. Koide, S. Yamasaki, S. Nagai, J. Umezaki, M. Koike, and M. Murakami, J. Appl. Phys. **81**, 1315 (1997).

[20] J. K. Sheu *et al.*, J. Appl. Phys. **83**, 3172 (1998).

[21] J.-K. Ho, C.-S. Jong, C.-N. Huang, C.-Y. Chen, C. C. Chiu, and K.-K. Shih, Appl. Phys. Lett. **74**, 1275 (1999).

[22] D. J. King, L. Zhang, J. C. Ramer, S. D. Hersee, and L. F. Lester, Mater. Res. Soc. Symp. Proc. **468**, 421 (1997).

[23] J. S. Jang, H. G. Kim, K. H. Park, C. S. Um, I. K. Han, S. H. Kim, H. K. Jang, and S. J. Park, Mater. Res. Soc. Symp. Proc. **482**, 1053 (1998).

[24] V. M. Bermudez, R. Kaplan, M. A. Khan, and J. N. Kuznia, Phys. Rev. B **48**, 2436 (1993).

[25] J. L. Richards and W. H. McCann, J. Vac. Sci. Technol. **6**, 644 (1969).

[26] H. Okamoto and T. B. Massalski, in *Alloy Phase Diagrams*, edited by T. B. Massalski, J. L. Murray, L. H. Bennett, and H. Baker (American Society for Metals, Metals Park, OH, 1990), p. 289.

[27] L. A. Grunes, R. D. Leapman, C. N. Wilker, R. Hoffmann, and A. B. Kunz, Phys. Rev. B **25**, 7157 (1982).

[28] C. Colliex, T. Manoubi, and C. Ortiz, Phys. Rev. B **44**, 11402 (1991).

[29] D. Adler, in *Solid State Physics*, edited by F. Seitz, D. Turnbull, and H. Ehrenreich (Academic, New York, 1968), p. 21.